Shape-Programmed Folding of Stimuli-Responsive Polymer Bilayers

Georgi Stoychev,[†,‡] Svetlana Zakharchenko,[†,‡] Sébastien Turcaud,[§] John W. C. Dunlop,[§] and Leonid Ionov[†,*]

[†]Leibniz Institute of Polymer Research Dresden, Hohe Straße 6, D-01069 Dresden, Germany and Department of Biomaterials, [‡]Technische Universität Dresden, Physical Chemistry of Polymer Materials, 01062 Dresden, Germany, and [§]Max Planck Institute of Colloids and Interfaces, Am Mühlenberg 1, D-14424, Potsdam, Germany

ABSTRACT We investigated the folding of rectangular stimuli-responsive hydrogel-based polymer bilayers with different aspect ratios and relative thicknesses placed on a substrate. It was found that long-side rolling dominates at high aspect ratios (ratio of length to width) when the width is comparable to the circumference of the formed tubes, which corresponds to a small actuation strain. Rolling from all sides occurs for higher actuation, namely when the width and length considerably exceed the deformed circumference. In the case of moderate actuation, when both the width and length are comparable to the deformed circumference, diagonal rolling is observed. Short-side rolling was observed very rarely and in combination with diagonal rolling. On the basis of experimental observations, finite-element modeling and energetic considerations, we argued that bilayers placed on a substrate start to roll from corners due to quicker diffusion of water. Rolling from the long-side starts later but dominates at high aspect ratios, in agreement with energetic considerations. We have shown experimentally and by modeling that the main reasons causing a variety of rolling scenarios are (i) non-homogenous swelling due to the presence of the substrate and (ii) adhesion of the polymer to the substrate.

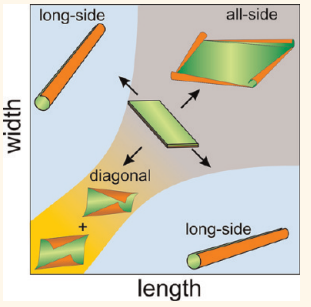

KEYWORDS: thermoresponsive · polymer · bilayer · tube · folding

Design of hollow 3D objects such as capsules and tubes is highly demanded for cell encapsulation, drug delivery and design of self-healing materials.[1] Most approaches for fabrication of capsules are based on the use of particles or fibers as templates, which are covered by functional materials. Hollow functional structures are, thus, formed after the removal of the core. Recently, the use of self-folding films that are able to form different 3D structures was suggested as a template-free alternative to the traditional template-based approaches.[2,3] The main advantage of self-folding films is the possibility to transfer a pattern, created on the surface of the unfolded film, into the inner and outer walls of the folded 3D structure.[4−6]

Inorganic and polymer-based bilayers are examples of self-folding films, which fold due to relaxation of internal stresses originated from dissimilar properties of the two layers, such as lattice mismatch, thermal expansion, or swellability. Inorganic-based self-folding films are promising for a variety of fields including transport,[7] nanooptics,[8] energy storage elements,[9] photovoltaic power applications,[10] optics,[11] and engineering of scaffolds,[12−15] as well as being suitable to investigate the role of confinement on cell behavior.[16] Polymer-based self-folding films, on the other hand, are particularly promising for biotechnological applications such as encapsulation of cells[17,18] and design of biomaterials.[19] These and other applications require precise control of the folding for fabrication of 3D objects with a defined shape. In particular, it was demonstrated that the resulting shape of the folded 3D object can be controlled by the shape of the original bilayer. For example, rectangular bilayers form tubes,[17] while star-like bilayers are able to form envelope-like capsules.[18]

Generally, the rolling of a rectangular bilayer may occur according to three different scenarios: long-side, short-side, and diagonal rolling (see Figure 1). The effects of film shape on the character of folding were experimentally investigated on examples of purely inorganic and composite polyaniline−inorganic bilayers. Smela *et al*. showed that short-side rolling was preferred in the case of free homogeneous actuation and that this preference increased with aspect ratio (ratio of length to width of rectangular pattern).[20] Li *et al*. experimentally demonstrated the opposite scenario[21] in the case where bilayers are progressively etched from a substrate, namely a preference for long-side rolling. They observed that when the tube circumference was much larger than the width, or the aspect ratio of the rectangle was high, rolling always occurred from the long side. When the tube circumference was much smaller than the width

* Address correspondence to ionov@ipfdd.de.

Received for review January 7, 2012 and accepted April 24, 2012.

Published online April 24, 2012
10.1021/nn300079f

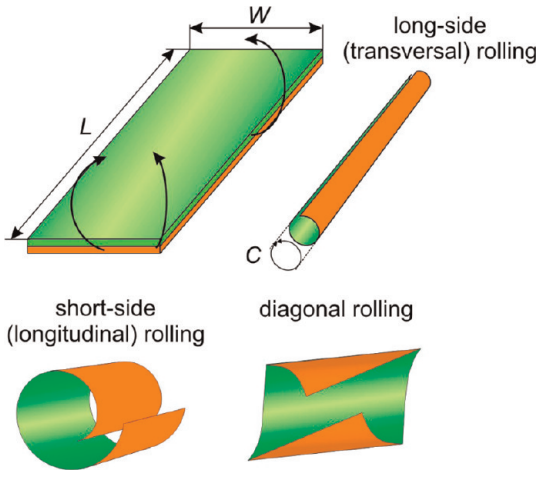

Figure 1. Scheme of rolling of a polymer bilayer according to different scenarios: short-side, long-side, and diagonal rolling.

and the aspect ratio of the rectangular bilayer was not very high, the rolling resulted in a mixed yield of long- and short-side rolling, as well as a "dead-locked turnover" shape. Short-side rolling occurred at small aspect ratios when the deformed circumference is close to the width. In these self-rolling systems, the active component undergoes relatively small volume changes or actuation strains, which are nearly homogeneous over the whole sample. Hydrogel films, which are also able to fold, demonstrate considerably different properties.[22−24] First, hydrogels undergo large volume changes (up to 10 times) upon swelling and contraction. Second, the swelling of a hydrogel is often kinetically limited: due to slow diffusion of water through a hydrogel, the parts that are closer to the edges swell first, while the parts that are closer to the center of the films swell later. Thus, the actuation profile inside the active layer is heterogeneous. In this paper we investigate the effects of shape, size, and rolling curvature on the direction of folding of rectangular polymer bilayers placed on a substrate, where the bottom component is a stimuli-responsive hydrogel.

EXPERIMENTAL OBSERVATIONS

Experimental Preparation. Two families of polymeric bilayers, made of an active and a passive layer, are studied. The passive component is either hydrophobic polycaprolactone (PCL) or random copolymer poly(methylmethacrylate-*co*-benzophenone acrylate) (P(MMA-BA)). The active component is a thermoresponsive hydrogel formed either by photo-cross-linked poly(*N*-isopropylacrylamide-*co*-acrylic acid-*co*-benzophenone acrylate) (P(NIPAM-AA-BA)) or by poly(*N*-isopropylacrylamide-*co*-benzophenone acrylate) (P(NIPAM-BA)). Thermoresponsive hydrogels swell and shrink at reduced and elevated temperature, respectively. The passive hydrophobic P(MMA-BA) and PCL layers restrict swelling of the active hydrogel. As a result, the bilayer made of these polymers does not uniformly expand/shrink but folds and unfolds due to swelling and collapse of the hydrogel layer.

P(NIPAM-AA-BA)/(P(MMA-BA) and P(NIPAM-BA)/PCL bilayers were prepared using photolithography, as described earlier.[17] First, we prepared two sets of patterned bilayers of P(NIPAM-AA-BA)/(P(MMA-BA), which differ in thickness (H) of the P(MMA-BA) layer, which results in different rolling curvature. One set formed narrow tubes with a diameter d = 20 μm ($H_{P(MMA-BA)}$ = 500 nm; $H_{P(NIPAM-AA-BA)}$ = 1200 nm), while the second set forms wider tubes with diameters in the range d = 70−90 μm ($H_{P(MMA-BA)}$ = 1200 nm; $H_{P(NIPAM-AA-BA)}$ = 1200 nm). Rectangular bilayers of different lengths (L = 100−1000 μm) and aspect ratios (ratio of length (L) to width (W), $A = L/W$ = 1−8) were fabricated using specially designed photomasks. After removal of the non-cross-linked polymer, the patterned bilayers were exposed to PBS solution (pH = 7.4) at room temperature. As a result, photo-cross-linked P(NIPAM-AA-BA) swelled, leading to rolling of the bilayer and formation of tubes. The folded films formed by each set of bilayers were then mapped by optical microscopy in order to assess the rolling radius as well as the deformation pattern (see Figures 2 and 3).

Experimental Results. It was found that the final diameter of the tube is independent of the size of the bilayer (L, W), but everything else being equal (Young modulus of active and passive layer as well as activation strain), it is solely controlled by the relative thickness of the active and passive layers[25] and, thus, is (almost) constant for each set of experiments. The direction of rolling strongly depends on the size and shape of the films as well as on the thickness of the active and passive layer (see Figure 4). We distinguished four general types of rolling: long-side rolling, diagonal rolling, short-side rolling, and mixed all-side rolling, which is a combination of the first three types. The character of preferential rolling is plotted as a function of the absolute values of width, length, and aspect ratio, as well as normalized values, which are obtained by dividing the length or width by the typical circumference of the rolled tube ($C = \pi d$, Figure 1).

Three types of rolling were observed when narrow tubes (d = 20 μm) are formed: long-side, diagonal, and all-side rolling (see Figure 4a). It must be noted that no short-side rolling was observed. The all-side rolling (see Figure 2, a1−3, b1−2) occurs when the width of the films considerably exceeds the circumference of rolling for aspect ratios of 1 or 2. A decrease of the width for an aspect ratio of 2 or more results in preferential long-side rolling (see Figure 2, b3, c1−3, d1−3), when the normalized length is more than 2. Depending on the ratio of width (W) to circumference (C), incompletely rolled tubes ($W/C < 1$), completely rolled tubes ($W/C \approx 1$), or doubled tubes ($W/C \geq 2$) are formed. A further decrease of the length leads to a mixture between

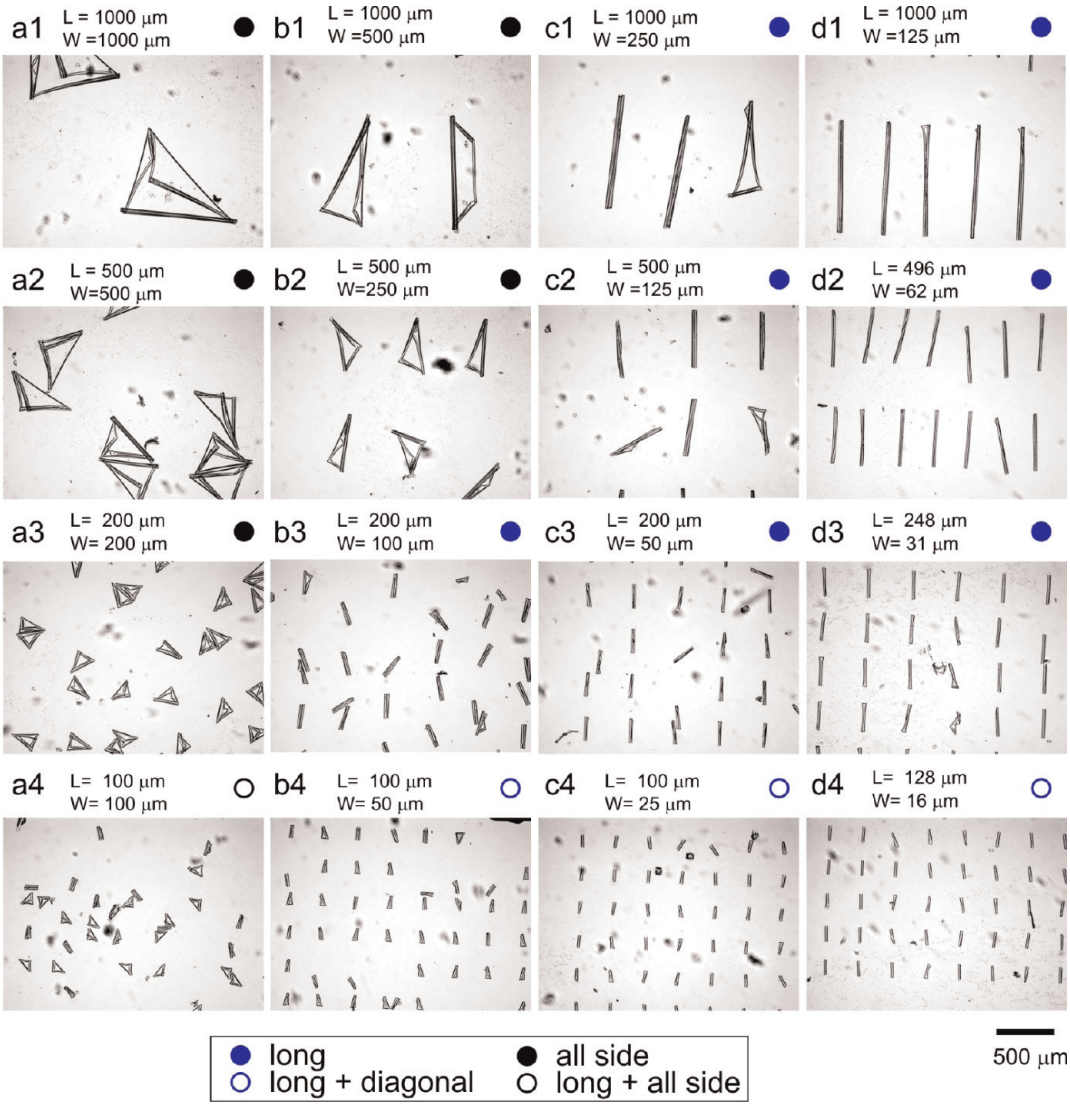

Figure 2. Microscopy snapshots of folded P(NIPAM-AA-BA)−P(MMA-BA) bilayers of different length (*L*) and width (*W*) that form narrow tubes of diameter $d = 20\ \mu m$; $H_{P(MMA\text{-}BA)} = 500$ nm; $H_{P(NIPAM\text{-}AA\text{-}BA)} = 1200$ nm.

long-side and diagonal or all-side rolling (see Figure 2, a4, b4, c4, and d4). The most promising parametric window for potential applications, such as microfluidics[24] and cell encapsulation,[17] is thus bilayers with an aspect ratio of 4 or more.

Different rolling behavior is observed when wide tubes ($d = 70-90\ \mu m$) are formed (see Figure 4b). First, the films with the highest aspect ratio slightly bend and almost do not roll because of the large circumference (see Figure 3, d1−4). Second, other bilayers roll either according to diagonal or all-side rolling scenarios. Diagonal rolling is observed in the cases of square films ($L/W = 1$) when two opposite corners bend toward each other (see Figure 3, a1−4). "Tick or check mark-like" structures (see for example Figure 3, c1, the film in the middle) in combination with diagonal rolling are observed in almost all cases at $L/W > 1$ when either adjacent or opposite corners bend toward each other. Bending from short sides was observed in combination with diagonal rolling only in one case (see Figure 3, b4).

The results obtained for narrow (Figure 2 and 4a) and wide (Figure 3 and 4b) tubes plotted as a function of normalized length and width are not fully identical. Figure 4b is shifted to larger values of *L*/*C*. The reason for this effect is not completely clear and could be due to effects related to heterogeneities in the swelling behavior, which are hard to fully consider. On the other hand, there is a clear correlation between the results given in Figure 4a and b, which is qualitatively summed up in Figure 4c. For example, all-side rolling is observed when both length and width considerably exceed the deformed circumference. Diagonal rolling is observed when $L = W$, and both are comparable to the circumference. Mixtures of diagonal rolling and the formation of "tick or check mark-like" structures (tube in the middle of Figure 3, c1) are observed when $L > W$ and both *L* and *W* are comparable to the circumference.

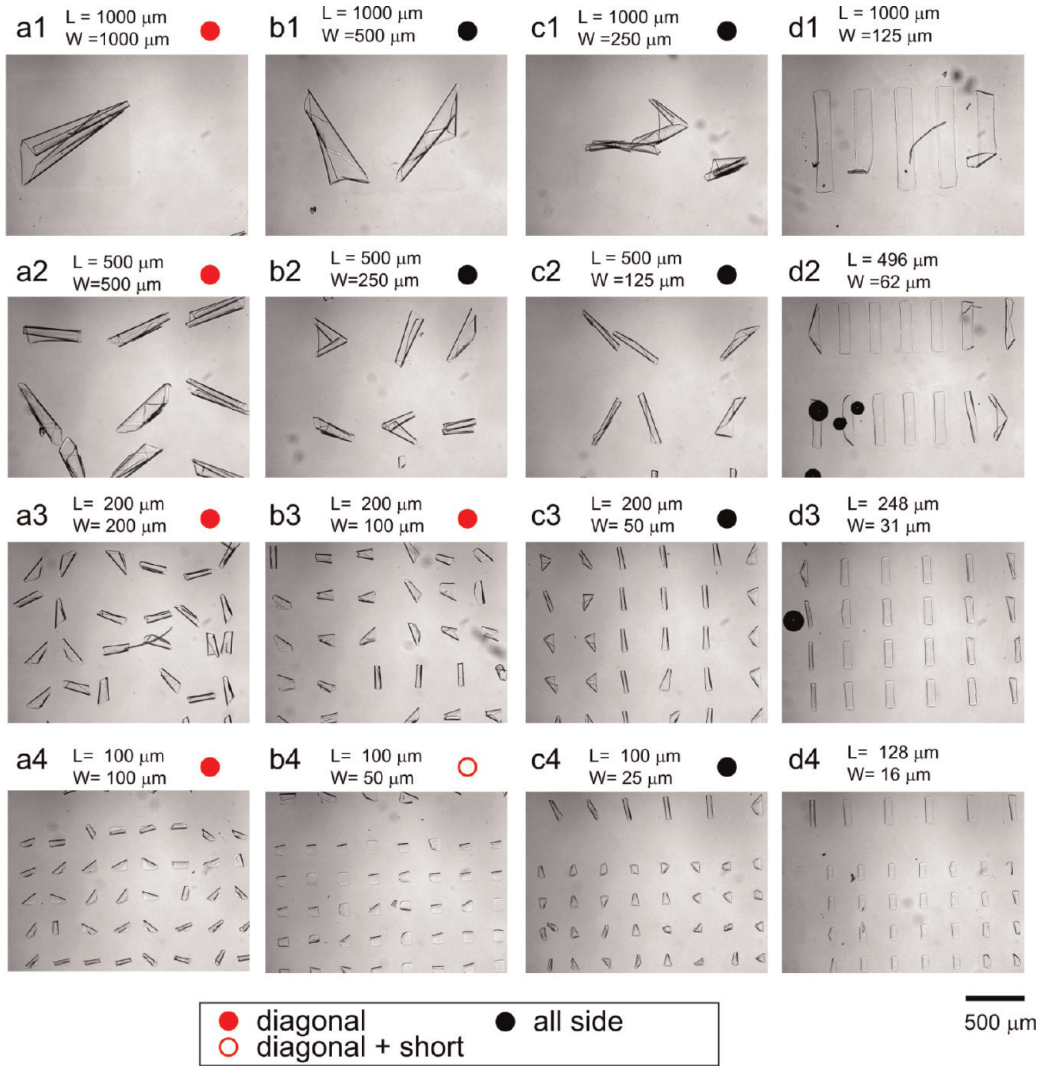

Figure 3. Microscopy snapshots of folded P(NIPAM-AA-BA)−P(MMA-BA) bilayers with different length (*L*) and width (*W*) that form wide tubes of diameter $d = 70-90\ \mu m$; $H_{P(MMA-BA)} = 1200$ nm; $H_{P(NIPAM-AA-BA)} = 1200$ nm.

The long-side rolling takes place when the length considerably exceeds the deformed circumference ($L/C > 4$) and the aspect ratio is larger than 4. As a result, long tubes are formed, at least in the case of narrow tubes ($d = 20\ \mu m$). In order to test the hypothesis that long tubes are formed when $L/C > 4$ and $W \approx C$ also in the case of wide tubes ($d = 70-90\ \mu m$), we investigated rolling of 1800 $\mu m \times 300\ \mu m$ large bilayer tubes ($H_{P(MMA-BA)} = 1200$ nm, $H_{P(NIPAM-AA-BA)} = 1200$ nm, $W/C = 1.2$; $L/C = 7.5$). Indeed, rolling resulted in preferential formation of long tubes (see Figure 4d), in agreement with our predictions.

Mechanism of Rolling. In order to clarify the variety of observed rolling scenarios, we experimentally investigated swelling and rolling of the bilayers. Rolling was investigated first using members of the second family of patterned bilayers formed by poly(*N*-isopropylacrylamide-*co*-benzophenone acrylate) and polycaprolactone with high aspect ratio ($L/W = 6$, $H_{PCL} = 300$ nm, $H_{P(NIPAM-BA)} = 750$ nm).[17] Initially, the polymer films were immersed in warm water, where the active P(NIPAM-BA) hydrogel monolayer is shrunk. The temperature was gradually decreased, and rolling was observed. Diagonal rolling started from corners and stopped when two rolling fronts met each other (Figure 5a). Long-side rolling started later (Figure 5b) but eventually dominated, leading to a switching of the diagonally rolled corners to long-side rolled (Figure 5c,d). The formed double tubes were unrolled at elevated temperature (Supporting Information, Movie S1). The central part of the rolled bilayer, which has a shape of a line (Figure 5e), is still adhered to the substrate after rolling because the bilayer remains almost undeformed there. This adhesion area directs long-side rolling during the second cycle of temperature decrease and prevents short-side rolling. The second rolling, thus, proceeded similar to the first one: rolling starts from the corners and then switches to long-side rolling.

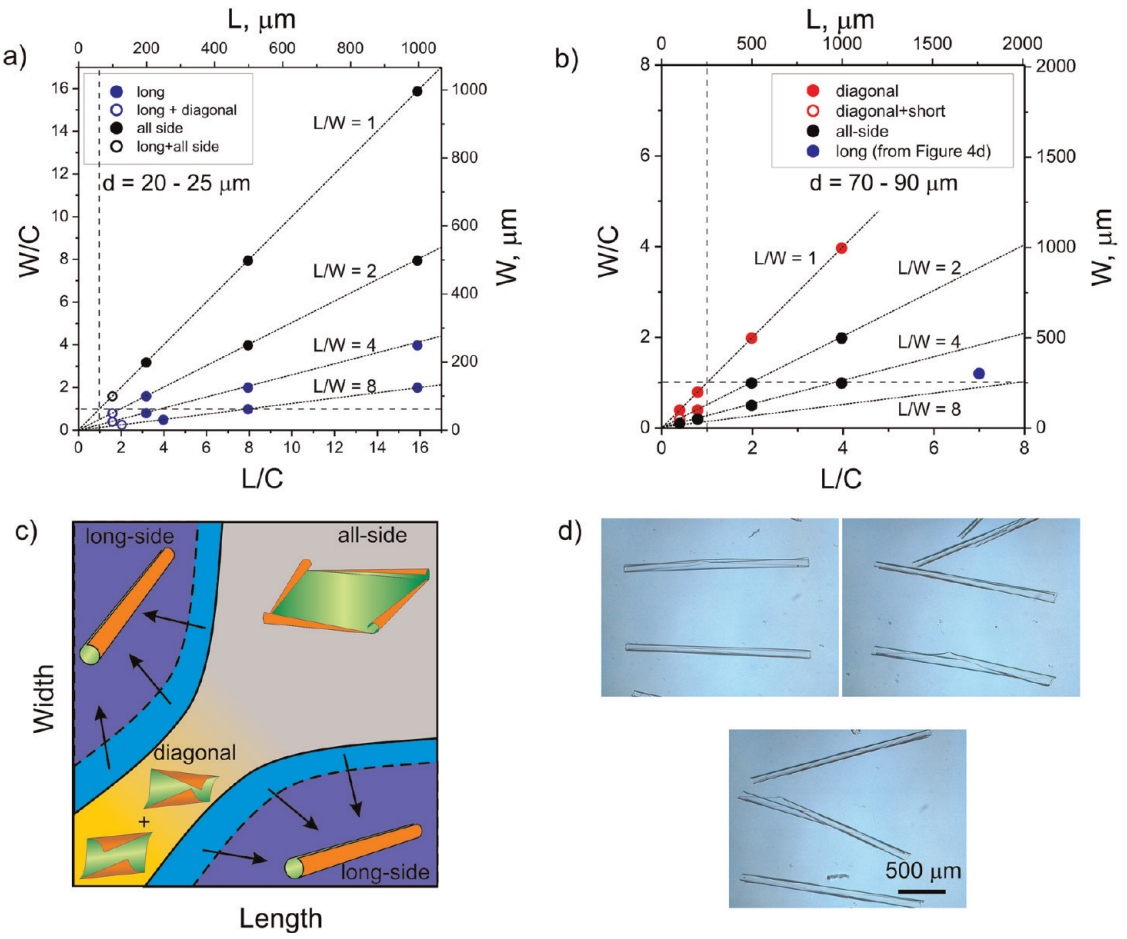

Figure 4. Dependence of preferential rolling direction of P(NIPAM-AA-BA)−P(MMA-BA) bilayers on the size and shape of the films when (a) narrow (d = 20 μm, $H_{P(MMA-BA)}$ = 500 nm; $H_{P(NIPAM-AA-BA)}$ = 1200 nm) and (b) wide (d = 70−90 μm, $H_{P(MMA-BA)}$ = 1200 nm; $H_{P(NIPAM-AA-BA)}$ = 1200 nm) tubes are formed. Dashed lines correspond to L/C = 1 and W/C = 1 (L and W are length and width of the film, respectively; C is the circumference of the rolled tube). (c) Schematic diagram of rolling scenario as a function of length and width. Arrows indicate how the diagram changes when circumference (C) increases. (d) Examples of wide tubes (d = 80 μm, $H_{P(MMA-BA)}$ = 1200 nm; $H_{P(NIPAM-AA-BA)}$ = 1200 nm) formed by rolling of 1800 μm × 300 μm large bilayers (corresponds to the blue point in part b).

In order to explain the fact that rolling starts from the corners, we experimentally investigated the swelling process. This was performed in a qualitative manner by observing changes in the interference pattern of white light with the bilayer during swelling. In order to avoid bending and folding of the bilayer during swelling, a very thin P(NIPAM-AA-BA) layer (H = 35 nm) under a thick P(MMA-BA) layer (H = 400 nm) was used. Due to the effect of interference of light, which is mirrored from the top and bottom surfaces of the bilayer, the changes of colors (see Figure 6) reflect changes in the film thickness. It is observed that the color of the films starts to change at the corners first, which confirms the assumption that edge-activation of the active layer due to slow water diffusion into the hydrogels is at the origin of the experimentally observed fact that rolling starts at corners. Thus, on the basis of the observations of rolling and swelling mechanisms, we can argue that diffusion determines folding in the first moments of folding, while adhesion seems to play a decisive role at later stages of folding.

THEORETICAL CONSIDERATIONS

Diffusion-Driven Actuation. The observed long-side folding of rectangular bilayers for some specific shape parameters contradicts the bending of bilayer actuators, which occurs along the short side.[20,25] However, this holds under the assumption that the active layer is homogeneously activated and that there is no interaction with a substrate. This is the case of a freely floating bilayer, where diffusion of water inside the hydrogel layer is not restricted by any substrate. It was confirmed that such freely floating bilayers undergo short-side rolling that is similar to the behavior of standard actuators (Figure 7a). As the studied bilayers are placed on a substrate, it is reasonable to assume that diffusion of water inside the active monolayer upon activation (T < T_critic) occurs primarily through its lateral sides. Additionally, not only does the substrate

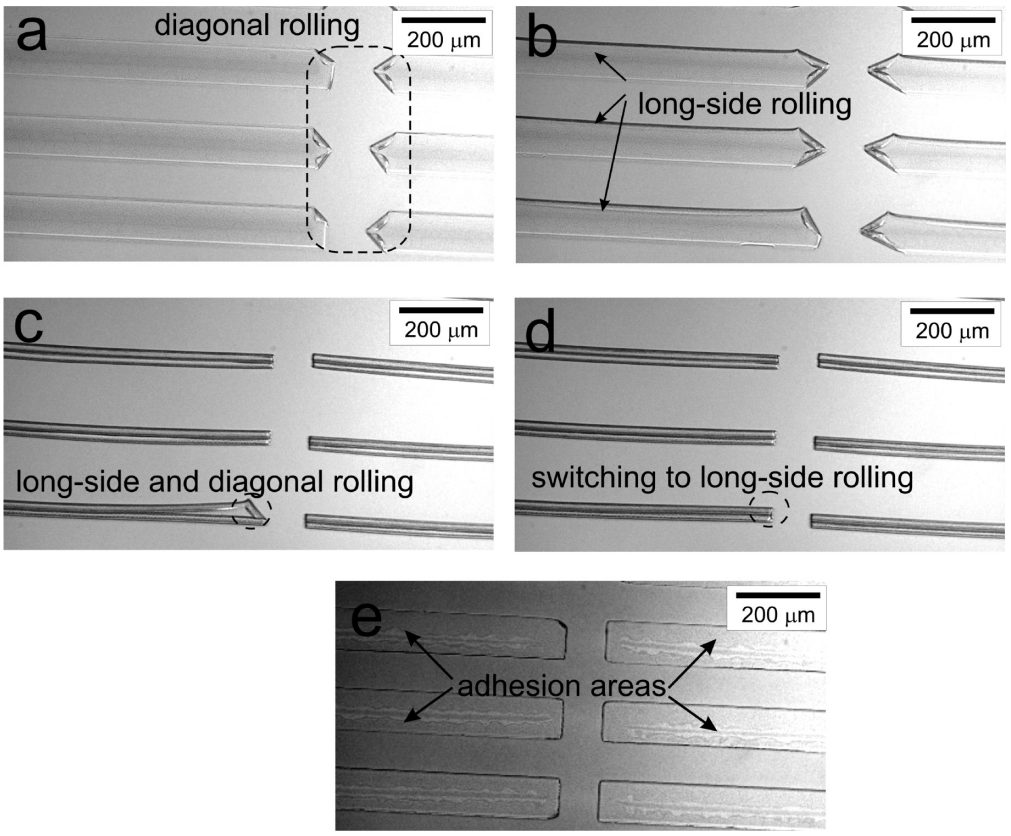

Figure 5. Time-resolved rolling of the P(NIPAM-BA)—PCL bilayer (H_{PCL} = 300 nm, $H_{P(NIPAM\text{-}BA)}$ = 750 nm, 930 μm × 90 μm); diameter of the tube d = 41 μm (a—e, supplementary Movie S1).

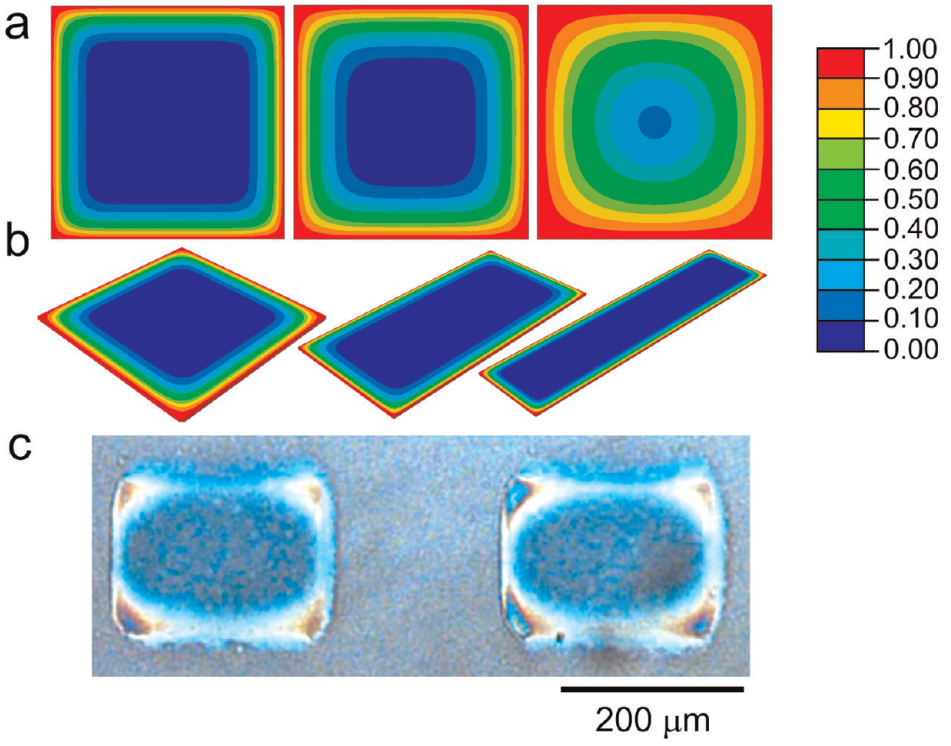

Figure 6. Color map of the calculated swelling (from 0 to 1) controlled by water diffusion in the active monolayer with a lateral constant boundary condition (blue is nonswollen) dependent on time (a) and shape (b) obtained by finite-element simulations as well as experimentally obtained microscopy snapshot of swollen P(NIPAM-BA)—PMMA bilayer ($H_{P(MMA\text{-}BA)}$ = 400 nm; $H_{P(NIPAM\text{-}AA\text{-}BA)}$ = 35 nm) after few seconds of swelling (c).

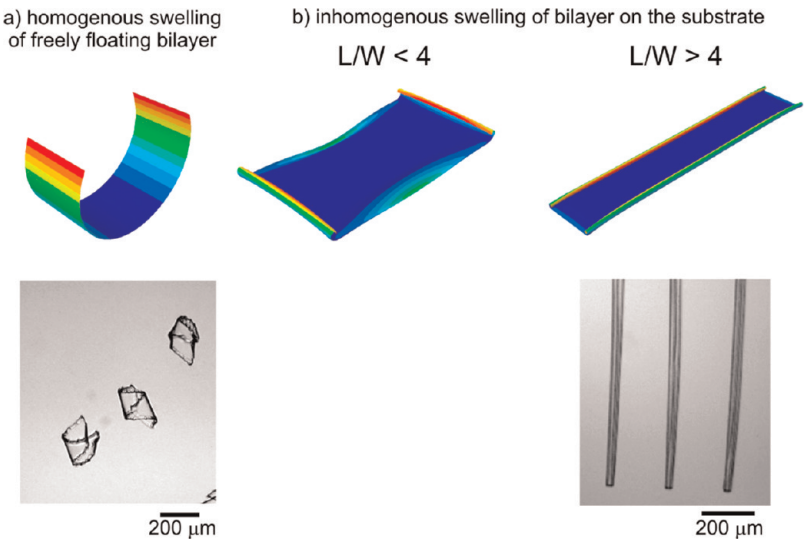

Figure 7. Simulation and experimentally observed folding of rectangular bilayers at different conditions: (a) freely floating rectangular bilayer (homogeneous swelling, supplementary Movie S2); (b) rectangular bilayer on substrate (inhomogeneous swelling, supplementary Movie S1).

confine diffusion, it also exerts adhesion forces to the bottom surface of the bilayer that impede actuation until a certain threshold of detachment forces is reached. This means that bending, which requires detachment of the substrate, occurs only for a sufficient activation strain. In particular, nonswollen areas do not bend.

Finite-Element Simulations. The diffusion pattern is assumed to obey a classical diffusion law (Fick's law) with a constant imposed boundary condition on the lateral sides of the active monolayer. Well known in one dimension, the two-dimensional diffusion pattern was obtained through a finite-element simulation using ABAQUS at different time points for different monolayer shapes (aspect ratio). Diffusion of water inside a hydrogel can be described as a first approximation by steady-state heat diffusion inside a medium with constant diffusivity. We used linear three-dimensional diffusion elements (DC3D8), in order to be able to apply the resulting activation field to actuate bilayers subsequently, and applied a constant boundary condition on the lateral surfaces. The solvent diffusion, however, is a very complex process that is quite difficult to fully describe because the boundary conditions of diffusion change as the film deforms and detaches from the substrate. We aimed to discuss diffusion in the very first moments of swelling, when the film starts to deform, as we believe that subsequent deformation of the film is largely determined by its starting deformation. The simulation allowed us to predict an inhomogeneous two-dimensional diffusion pattern that eventually becomes homogeneous after a sufficient time (see Figure 6a,b).

Subsequently, we applied the obtained thermal field at different time points to a bilayer of the same aspect ratio. Both layers of the bilayer are made of a linear elastic material with a normalized Young modulus of 1 and a Poisson ratio of 0.3. This crude simplification relies on the fact that the stiffness contrast between the active and the passive layer does not significantly affect the rolling radius of a bilayer.[25] The bottom layer possesses in-plane thermal expansion coefficients equal to 1, whereas the top layer is thermally inactive. In order to understand the influence of substrate adhesion, we imposed a fixed kinematical boundary condition at an internal rectangular bottom surface, scaled from the external shape. We used a fine mesh of first-order eight-node elements with reduced integration (C3D8R), which are able to follow the large displacements at reasonable cost. The deformed shape corresponding to an edge activation of the bilayer at a given time point in the diffusion process was calculated in a static step taking nonlinear geometric effects into account. Adaptive meshing techniques were used to avoid large distortions in mesh elements upon actuation. We compared the obtained results with the one obtained using the Riks method and found no discrepancy between the predicted deformed shapes. Surprisingly, convergence using a combination of adaptive meshing techniques on a fine mesh with a static nonlinear geometric step proved to be better than using the Riks method. This simple uncoupled model already shows that sharp activation strains near the edges combined with an internal constraint of the bottom layer produces interesting deformation patterns for different aspect ratios. In particular, the model predicts that short- and long-side rolling is more favorable at $L/W < 4$ and $L/W > 4$, respectively (see Figure 7b).

The appearance of all-side and diagonal rolling in experiments at smaller aspect ratios accounts for the fact that no preferential direction appears for bending

deformations. Also, imperfections of the material properties of the polymer film and substrate can be responsible for the observed symmetry-breaking.

Energetic Considerations. The fact that edge activation of a constrained bilayer leads to long-side rolling is also suggested by plate theory. The elastic energy of plate-like objects can be decomposed into a stretching and a bending term according to Föppl von Kármán plate theory,[26] in which the in-plane strains are integrated over the thickness taking into account the edge activation. This formulation describes accurately the elastic energy of a bilayer plate upon edge activation and can be solved numerically (this will be done in a subsequent paper). Another approach, which is less subtle, but that also leads to accurate results, is solving the 3D mechanical problem by a finite-element method. Essentially the problem can be described in the following way: we make an additive decomposition of the total strain in the active layer into an eigenstrain (or swelling strain) and an elastic strain $\varepsilon_{kl}^{T} = \varepsilon_{kl}^{eig} + \varepsilon_{kl}^{el}$. The eigenstrain is given as $\varepsilon_{ij}^{eig} = \alpha\delta_{ij}$, where δ_{ij} is the Kronecker delta tensor, and isotropic swelling is assumed in the current model. The amount of swelling depends on the swelling coefficient α, which in turn can vary spatially according to the solution of the diffusion equation. As the active layer is constrained by the passive layer, geometric incompatibilities result in elastic strains and thus stresses through Hooke's law, $\sigma_{ij} = E_{ijkl}\varepsilon_{kl}^{el}$. The final shape of the structure upon changes in the spatial distribution and magnitude of α is calculated by minimizing the elastic energy of the system. For further details of the finite-element method see, for example, ref 27. With the stretching term being linear in thickness, while the bending term is cubic, bending deformations are favored when the plate is sufficiently thin. Unlike in a beam-like bilayer, actuation triggers a biaxial expansion field inside the plate, which creates internal stresses in the long and in the short direction of the plate. Relaxation of internal stresses perpendicular to the edge of the bilayer will lead to bending, whereas relaxation of internal stresses parallel to the edge of the bilayer will produce stretching that will eventually lead to wrinkling, as in the edge of long leaves.[28] Because of the presence of the substrate, internal stresses perpendicular to the edge of the bilayer are more easily relaxed, leading to simple bending, while internal stresses parallel to the edge of the bilayer produce simple stretching. As the aspect ratio increases, it is thus less costly to relax stresses into bending on the long side than on the short side. This explains qualitatively why long-side rolling is observed as the aspect ratio increases.

Finite-element modeling and energetic considerations show that the experimentally observed appearance of long tubes for large aspect ratios and high activation strains are due to (i) non-homogenous swelling due to slow lateral diffusion, as well as (ii) adhesion of the bilayer to the substrate, constraining the deformations. Both these factors are caused by the specific arrangement of the experiment: (i) polymer bilayer is deposited on the substrate and (ii) active polymer is the bottom layer.

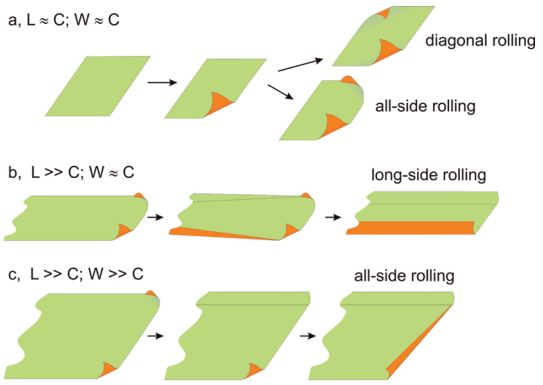

Figure 8. Schematic of rolling leading to diagonal rolling, long-side rolling, and all-side rolling.

Rolling Scenario. Finally, by considering modeling and experimental results, the following scenario of rolling of hydrogel-based polymer bilayer lying on a substrate is assigned. The rolling starts from the edges due to faster diffusion of water from the lateral surfaces, which then are able to detach from the substrate and to bend. Rolling can start either from two adjacent (for example Figure 3, d2, right lower polymer film, or Figure 3, b2, left upper film) or opposite edges (almost all polymer films in Figure 2, a2) or from all corners simultaneously, which is less probable if the bilayer is small due to the presence of imperfections and becomes energetically unfavorable once a sufficient actuation strain is reached. Rolling is almost immediately finished if the deformed circumference is comparable to the size of the bilayer. As a result, diagonally rolled tubes are formed if rolling starts from two opposite corners (Figure 8a), and "tick or check mark-like" structures (for example Figure 3, c1, the film in the middle) are formed if rolling starts from two adjacent corners.

A more complicated scenario is observed when the width of the films is smaller and the length is considerably larger than the deformed circumference. Rolling starts at the corners first, like before, but long-side rolling starts later (Figure 8b and Figure 5) and is energetically favored. Rolling along the short side is unfavorable because it implies more stored stretching energy along the long side. Further long-side rolling makes diagonally rolled corners unfavorable and leads to the switching of bent corners to a "long-side rolling" scenario. Depending on the width of the film compared to the deformed circumference, either an incompletely rolled tube is formed or the two long-side rolling fronts collide into a completely rolled or doubled tube.

If the deformed circumference is considerably smaller than the width and length of the films

(which implies a high activation strain), then rolling starts first from corners and then continues along all sides (Figure 8c). The rolling fronts do not collide until several revolutions are made, which were shown to be almost irreversible.[17] As a result, already rolled fronts are unable to unroll and irreversible all-side rolling is observed.

CONCLUSIONS

We investigated in detail folding of rectangular stimuli-responsive hydrogel-based polymer bilayers located on a substrate with different lengths, widths, and thicknesses. It was found that long-side rolling dominates at high aspect ratios (ratio of length to width) when the width is comparable to the circumference of the formed tubes. Rolling from all sides occurs when the width and length considerably exceed this circumference. Diagonal or all-side rolling is observed when the width and length are comparable to the circumference. Short-side rolling was observed very rarely and in combination with diagonal rolling. On the basis of both experimental observations and theoretical assumptions, we argued that bilayers placed on a substrate start to roll from corners due to quicker diffusion of water. Rolling from long-side starts later but dominates at high aspect ratio due to energetic considerations. We have shown experimentally and by finite-element modeling confirmed by theoretical considerations that the main reasons causing a variety of rolling scenarios are (i) non-homogenous swelling due to slow diffusion of water in hydrogels and (ii) adhesion of polymer to a substrate until a certain threshold. Moreover, non-homogenous swelling determines folding in the first moments, while adhesion plays a decisive role at later stages of folding.

The films that we investigated are fabricated on the microscale. On the other hand, the knowledge obtained in this work is applicable to thinner films to direct their folding in order to form tubes with diameter in the nano range. We believe that the obtained knowledge can be particularly helpful for the design of self-folding objects with highly complex shapes and provides an interesting model system for path-dependent actuation.

EXPERIMENTAL PART

Materials. *N*-Isopropylacrylamide (NIPAM, Aldrich), 4-hydroxybenzophenone (Fluka), polycaprolactone (M_n = 70 000–90 000, Aldrich), benzophenone (Aldrich), and acryloyl chloride (Fluka) were used as received. Methyl methacrylate (MMA, Alrich) was purified by filtration through an Al_2O_3 column before polymerization.

Synthesis of 4-Acryloylbenzophenone (BA). 4-Hydroxybenzophenone (20 g, 0.1009 mol), diisopropylethylamine (19.3 mL, 0.1110 mol), and 80 mL of methylene chloride were added into a 200 mL three-necked round-bottom flask fitted with an overhead stirrer, a thermometer, and an addition funnel with acroloyl chloride (9.02 mL, 0.1110 mol) solution in 20 mL of methylene chloride. The acroloyl chloride solution was added dropwise into the flask under cooling (0–5 °C) for *ca.* 3 h. The methylene chloride was removed by rotary evaporation. The residue was washed with 80 mL of 20% HCl and 80 mL of a saturated solution of sodium hydrocarbonate and dried over sodium sulfate. The solution was passed through a silica gel column with chloroform as the eluent. Chloroform was removed by rotary evaporator. Finally, 24.44 g (95%) of BA was obtained. ^{1}H NMR ($CDCl_3$, 500 MHz): 6.05 (dd, J_1 = 10.40, J_2 = 1.26, 1H), 6.34 (dd, J_1 = 10.40, J_3 = 17.34, 1H), 6.64 (dd, J_3 = 17.34, J_2 = 1.26, 1H), 7.27 (m, 2H), 7.49 (m, 2H), 7.59 (m, 1H), 7.80 (m, 2H), 7.86 (m, 2H).

Synthesis of P(NIPAM-BA). BA (0.02253 g, 0.089 mmol; 0.04551 g, 0.18 mmol; 0.11737 g, 0.47 mmol), NIPAM (1 g, 0.0885 mol), and azobisisobutyronitrile (AIBN) (0.01453 g, 0.089 mmol) were added in 10 mL test tubes. Components were dissolved in 6 mL of 1,4-dioxane and degassed with nitrogen for 30 min. Test tubes were tightly sealed and placed into a shaker (70 °C, 90 rpm) for 24 h. Then the P(NIPAN-BA) polymerization mixtures were cooled to room temperature and poured slowly into diethyl ether. Products were filtered and dried under vacuum.

Synthesis of P(MMA-BA). A 6.2803 g amount of MMA (62.72 mmol), 0.2405 g of BA (0.96 mmol), and 0.052 g of AIBN (0.31 mmol) were dissolved in 30 mL of toluene. The mixture was purged with nitrogen for 30 min. The polymerization was carried at 70 °C under a nitrogen atmosphere with mechanical stirring overnight. After cooling, the mixture was poured in 750 mL of diethyl ether, and the precipitate was filtered and dried under vacuum at 40 °C.

Preparation of Polymer Bilayers. In a typical experiment, poly(NIPAN-BA) was dip-coated from its ethanol solution on a silica wafer substrate. Polycaprolactone with 2–5 mass % of benzophenone or P(MMA-BA) was spin-coated from a toluene solution on poly(NIPAM-BA) film. The bilayer film was illuminated through a specially designed photomasks by a halogen lamp for 40 min to cross-link polymers. The illuminated film was rinsed in chloroform in order to remove polymers in nonirradiated areas.

Conflict of Interest: The authors declare no competing financial interest.

Acknowledgment. The authors are grateful to DFG (Grant IO 68/1-1) and IPF for financial support. We also thank Yves Bréchet for discussions about the FE simulations.

Supporting Information Available: Movies of long-side (Figure 5, S1) and short-side (Figure 7a, S2) rolling. This material is available free of charge *via* the Internet at http://pubs.acs.org.

REFERENCES AND NOTES

1. Esser-Kahn, A. P.; Odom, S. A.; Sottos, N. R.; White, S. R.; Moore, J. S. Triggered Release from Polymer Capsules. *Macromolecules* **2011**, *44*, 5539–5553.
2. Ionov, L. Soft Microorigami: Self-Folding Polymer Films. *Soft Matter* **2011**, *7*, 6786–6791.
3. Leong, T. G.; Zarafshar, A. M.; Gracias, D. H. Three-Dimensional Fabrication at Small Size Scales. *Small* **2010**, *6*, 792–806.
4. Randhawa, J. S.; Kanu, L. N.; Singh, G.; Gracias, D. H. Importance of Surface Patterns for Defect Mitigation in Three-Dimensional Self-Assembly. *Langmuir* **2010**, *26*, 12534–12539.
5. Luchnikov, V.; Sydorenko, O.; Stamm, M. Self-Rolled Polymer and Composite Polymer/Metal Micro- and Nanotubes with Patterned Inner Walls. *Adv. Mater.* **2005**, *17*, 1177–1182.
6. Cho, J. H.; Gracias, D. H. Self-Assembly of Lithographically Patterned Nanoparticles. *Nano Lett.* **2009**, *9*, 4049–4052.

7. Solovev, A. A.; Sanchez, S.; Pumera, M.; Mei, Y. F.; Schmidt, O. G. Magnetic Control of Tubular Catalytic Microbots for the Transport, Assembly, and Delivery of Micro-objects. *Adv. Funct. Mater.* **2010**, *20*, 2430–2435.
8. Smith, E. J.; Liu, Z.; Mei, Y. F.; Schmidt, O. G. System Investigation of a Rolled-Up Metamaterial Optical Hyperlens Structure. *Appl. Phys. Lett.* **2009**, *95*, 083104.
9. Bof Bufon, C. C. s.; Cojal González, J. D.; Thurmer, D. J.; Grimm, D.; Bauer, M.; Schmidt, O. G. Self-Assembled Ultra-Compact Energy Storage Elements Based on Hybrid Nanomembranes. *Nano Lett.* **2010**, *10*, 2506–2510.
10. Guo, X. Y.; Li, H.; Ahn, B. Y.; Duoss, E. B.; Hsia, K. J.; Lewis, J. A.; Nuzzo, R. G. Two- and Three-Dimensional Folding of Thin Film Single-Crystalline Silicon for Photovoltaic Power Applications. *Proc. Natl. Acad. Sci. U. S. A.* **2009**, *106*, 20149–20154.
11. Schwaiger, S.; Broll, M.; Krohn, A.; Stemmann, A.; Heyn, C.; Stark, Y.; Sticklerbhas, D.; Heitmann, D.; Mendach, S. Rolled-Up Three-Dimensional Metamaterials with a Tunable Plasma Frequency in the Visible Regime. *Phys. Rev. Lett.* **2009**, *102*, 163903.
12. Gracias, D. H.; Tien, J.; Breen, T. L.; Hsu, C.; Whitesides, G. M. Forming Electrical Networks in Three Dimensions by Self-Assembly. *Science* **2000**, *289*, 1170–1172.
13. Leong, T.; Gu, Z. Y.; Koh, T.; Gracias, D. H. Spatially Controlled Chemistry Using Remotely Guided Nanoliter Scale Containers. *J. Am. Chem. Soc.* **2006**, *128*, 11336–11337.
14. Randall, C. L.; Kalinin, Y. V.; Jamal, M.; Manohar, T.; Gracias, D. H. Three-Dimensional Microwell Arrays for Cell Culture. *Lab Chip* **2011**, *11*, 127–131.
15. Jamal, M.; Bassik, N.; Cho, J. H.; Randall, C. L.; Gracias, D. H. Directed Growth of Fibroblasts into Three Dimensional Micropatterned Geometries via Self-Assembling Scaffolds. *Biomaterials* **2010**, *31*, 1683–1690.
16. Huang, G. S.; Mei, Y. F.; Thurmer, D. J.; Coric, E.; Schmidt, O. G. Rolled-Up Transparent Microtubes as Two-Dimensionally Confined Culture Scaffolds of Individual Yeast Cells. *Lab Chip* **2009**, *9*, 263–268.
17. Zakharchenko, S.; Puretskiy, N.; Stoychev, G.; Stamm, M.; Ionov, L. Temperature Controlled Encapsulation and Release Using Partially Biodegradable Thermo-Magneto-Sensitive Self-Rolling Tubes. *Soft Matter* **2010**, *6*, 2633–2636.
18. Stoychev, G.; Puretskiy, N.; Ionov, L. Self-Folding All-Polymer Thermoresponsive Microcapsules. *Soft Matter* **2011**, *7*, 3277–3279.
19. Zakharchenko, S.; Sperling, E.; Ionov, L. Fully Biodegradable Self-Rolled Polymer Tubes: a Candidate For Tissue Engineering Scaffolds. *Biomacromolecules* **2011**, *12*, 2211–2215.
20. Alben, S.; Balakrisnan, B.; Smela, E. Edge Effects Determine the Direction of Bilayer Bending. *Nano Lett.* **2011**, *11*, 2280–2285.
21. Chun, I. S.; Challa, A.; Derickson, B.; Hsia, K. J.; Li, X. Geometry Effect on the Strain-Induced Self-Rolling of Semiconductor Membranes. *Nano Lett.* **2010**, *10*, 3927–3932.
22. Stuart, M. A. C.; Huck, W. T. S.; Genzer, J.; Muller, M.; Ober, C.; Stamm, M.; Sukhorukov, G. B.; Szleifer, I.; Tsukruk, V. V.; Urban, M.; *et al.* Emerging Applications of Stimuli-Responsive Polymer Materials. *Nat. Mater.* **2010**, *9*, 101–113.
23. Singamaneni, S.; McConney, M. E.; Tsukruk, V. V. Swelling-Induced Folding in Confined Nanoscale Responsive Polymer Gels. *ACS Nano* **2010**, *4*, 2327–2337.
24. Jamal, M.; Zarafshar, A. M.; Gracias, D. H. Differentially Photo-Crosslinked Polymers Enable Self-Assembling Microfluidics. *Nat. Commun.* **2011**, *2*, 527.
25. Timoshenko, S. Analysis of Bi-Metal Thermostats. *J. Opt. Soc. Am. Rev. Sci. Instrum.* **1925**, *11*, 233–255.
26. Audoly, B.; Pomeau, Y. *Elasticity and Geometry: from Hair Curls to The Non-Linear Response of Shells*; Oxford University Press: Oxford, 2010.
27. Zienkiewicz, O. C.; Taylor, R. L. *Finite Element Method for Solid and Structural Mechanics*, 6th ed.; Elsevier: New York, 2005.
28. Liang, H. Y.; Mahadevan, L. Growth, Geometry, and Mechanics of a Blooming Lily. *Proc. Natl. Acad. Sci. U. S. A.* **2011**, *108*, 5516–5521.